

Polymer complexes. LXXVIII. Synthesis and characterization of supramolecular uranyl polymer complexes: Determination of the bond lengths of uranyl ion in polymer complexes

M.A. Diab¹  | S.G. Nozha² | A.Z. El-Sonbati¹  | M.A. El-Mogazy¹ | Sh.M. Morgan³ 

¹Chemistry Department, Faculty of Science, Damietta University, Damietta, Egypt

²Domyat Laboratory, Ministry of Health, Damietta, Egypt

³Environmental Monitoring Laboratory, Ministry of Health, Port Said, Egypt

Correspondence

Sh.M. Morgan, Environmental Monitoring Laboratory, Ministry of Health, Port Said, Egypt.

Email: shimaa_mohamad2010@yahoo.com

The UO₂(II) polymer complexes (**1–5**) of azo dye ligands 5(4'-derivatives phenylazo)-8-hydroxy-7-quinolinecarboxaldehyde (HL_x) were prepared and characterized by elemental analysis, ¹H NMR, IR spectra, thermal analysis and X-ray diffraction analysis (XRD). The molecular geometrical structures and quantum chemical of the ligands (HL_x) and their tautomeric forms (**D** and **G**) were calculated. Molecular docking between the HL_x ligands and their tautomeric form with two receptors of the breast cancer (1JNX) and the prostate cancer (2Q7K) was discussed. From the histogram of the HOMO–LUMO energy gap (ΔE) and the estimated free energy of binding of the receptors of prostate cancer (2Q7K) and breast cancer (1JNX) for the ligands (HL_x), it is observed that the ΔE values of the ligands (HL_x) increases in the order HL₂ < HL₃ < HL₄ < HL₁ < HL₅. The electronic structures and coordination were determined from a framework for the modeling of the formed polymer complexes. From the IR spectra of the polymer complexes, the symmetric stretching frequency ν_3 values of UO₂²⁺ were used for the determination of the force constant (F_{U-O} (in 10⁻⁸ N/)) and the bond length (R_{U-O} ()) of the U–O bond by using Wilson, G. F. matrix method, McGlynn & Badger's formula and El-Sonbati equations. The plot of the bond distance r_{U-O} (r_1 , r_2 , r_3 , and r_t) vs. ν_3 was showed straight lines with increase in the value of ν_3 and decrease in r_{U-O} .

KEYWORDS

molecular docking, molecular geometrical structures, polymer complexes, quantum chemical parameters, thermal decomposition analyses

1 | INTRODUCTION

Literature surveys indicate that quinoline derivatives possess diverse pharmacological activities, including anti-inflammatory, antiviral, antitumor activities antimicrobial and, antibody titer against bovine respiratory syncytial (BRS) virus in serum neutralizations test (SNT).^[1–6] Also,

they have been used in chromatography and for the detection of metal ions, antioxidant and biological effect activities.^[7–9] The chemistry of transition metal complexes of 8-hydroxyquinoline has received much attention as their rational design and synthesis in coordination chemistry, also because of their potential applications as functional materials and in bioinorganic chemistry.

Quinolines compounds are considered as the major class of heterocyclics that are found in many biologically active natural products and synthetic molecules and quinoline derivative compounds are known to be the best chelating agents.^[5,10] They form very stable chelate rings with metal centers, and very stable complexes with a number of metal ions. The deprotonated oxygen atom and the ring nitrogen atom are involved in the metal chelation.^[5,6]

8-Hydroxyquinoline moiety has received considerable attention due to their efficient ionospheres, therapeutic and fluorescence properties.^[11–13] The parent aldehyde, 7-formyl-8-hydroxyquinoline, used in the present study as its azo dye derivative for the preparation of five asymmetrical azo dye ligands was previously used to prepare its own metal complexes. The coordination complexes of bivalent transition and non-transition metals was an interesting topic because of a Scaffold and supra-molecular skeleton, beautiful artistic, spectacular geometry, captivating functional property, and high thermal stability.^[14–18] Coordination chemistry of multidentate ligands with transition metals offers versatility attraction from supramolecular structures, functional aspects, and remarkable applications in the branch of solid state chemistry.^[19–24]

Polymer science was emerged as active branch of materials science. This field impinges on areas of commodity, engineering and specialty polymers thereby stimulating interest all over the globe in exploiting newer domains. This emerged branch is polymer metal complexes with organic polymer containing coordinating sites, complexed with metals. The research on coordination polymers has been constantly developed in past years. They have excellent properties as treatment of wastewater, semiconducting catalytic properties, in metal recovery, in protective coating, as antifouling paints and anti-fungal properties.^[10,25–27]

Uranyl polymer complexes of ligands (HL_x) are synthesized and characterized by using various spectroscopic techniques for identifying its structures and geometries. The geometrical studies of the ligands (HL_x) and their tautomeric forms are optimized theoretically. Molecular docking between form ligands (HL_x) and their tautomeric form with two types of proteins is studied. Study the relation between molecular geometrical structures and molecular docking. Determination the stretching and interaction force constants from which the U-O bond distances is calculated. Also, the thermal analysis data permit us to obtain information regarding the structure elucidation. The thermodynamic-kinetic parameters of polymer complexes are calculated by using the Coats-Redfern and Horowitz-Metzger methods to confirm the stability of them.

2 | EXPERIMENTAL

2.1 | Materials

All chemicals used in this study were of pure grade and of highest purity available were used without further purification. The chemicals used included aniline or *p*-substituted derivatives and 8-hydroxyquinoline (Sigma), UO₂(NO₃)₂·6H₂O and organic solvents included ethanol, methanol and dimethylformamide (DMF). were spectroscopically pure from BDH Chemical Ltd. Hydrochloric acid, sodium nitrite, sodium hydroxide, potassium hydroxide and sodium acetate (AR) were used without further purification. Elemental analyses (C, H, and N) were carried out at the Microanalytical Unit of Cairo University. The percentages of uranium content of each complex were determined by igniting a definite mass of the sample at 1000 °C and weighing the residue. Infrared spectra were recorded in the form of KBr discs using a Pye Unicam Sp 2000 spectrophotometer. ¹H NMR spectra were obtained on a JEOL Fx 900Q Fourier transform spectrometer using DMSO-d₆ as solvent and tetramethylsilane (TMS) as internal reference. The magnetic moment of the prepared solid complexes was determined at room temperature using Gouy method. Mercury (II) tetrathiocyanatocobalt (II) [Hg{Co(SCN)₄}], Diamagnetic corrections were calculated from the values given by Selwood^[28] using Pascal's constants. Thermal studies were performed on Simultaneous Thermal Analyzer (STA) 6000 and the thermal properties of the samples were carried out in the temperature range from 30 to 800 °C at the heating rate of 10 °C/min under dynamic nitrogen atmosphere. X-ray diffraction analysis of compounds was recorded on X-ray diffractometer analysis in the range of diffraction angle 2θ° = 4–80^[29–32] using CuK_α radiation. The tube applied voltage and current are 40 kV and 30 mA, respectively.

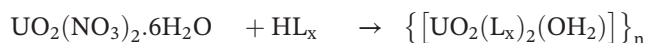
The molecules were built with Perkin Elmer ChemBio3D software^[30,33,34] and the quantum chemical parameters such as the highest occupied molecular orbital energy (E_{HOMO}), the lowest unoccupied molecular orbital energy (E_{LUMO}) and HOMO-LUMO energy gap (ΔE*) for the tautomeric forms (**A**, **D** and **G**) of the ligands (HL_x) were calculated. The El-Sonbati equation was manipulated using a computer program developed in our laboratories using the C Language. Molecular docking calculations of the binding between the receptors of the breast cancer (IJNX Gene regulation) and the prostate cancer (2Q7K Hormone) protein models were carried out. The MMFF94 Force field was used for energy minimization of the ligand molecules using Docking Server.^[34–36] Auto Dock parameter set- and distance-dependent dielectric functions were used in the calculation of the van der Waals and electrostatic terms.

2.2 | Synthesis of the ligands (HL_x)

Aniline or *p*-substituted derivatives (1 mmol) (1a) was dissolved in 30 ml of ethanol. Concentrated hydrochloric acid (10 ml) was diluted with about 40 g of crushed ice and then dropwise addition of the aniline or *p*-substituted derivatives solution to the crushed ice.^[15,17] To this cold solution addition of 10% sodium nitrite (1 mmol) and stirred for about 1 hr to complete diazotization (2a). The coupling agent 8-hydroxy-7-quinolinecarboxaldehyde (1 mmol) (3a) dissolved in 50 ml of ethanol containing (1.0 mmol) of potassium hydroxide was then added to the cold mixture. The resulting solution was stirred well and sodium acetate (3 g) was added for neutralization. The ligands (HL_x) were washed with ethanol and col-

lected by filtration and washed with a cold water-methanol mixture to remove the unreacted uranyl salts, followed by overnight vacuum drying. The purity of the formed polymer components was examined by TLC to confirm the reaction of the ligands with UO₂(NO₃)₂·6H₂O. The inherent viscosities ($\eta_{inh} = \ln r/C$; C = 0.5 g dl⁻¹) measured with a Desreux-Bishoff suspended level viscometer at 30 °C ± 0.001 °C, using dimethylsulphoxide (DMSO) as solvent are found to be in the range 1.35–1.54 for the polymer complexes (1–5), respectively. The analytical data of all polymer complexes are collected.

The polymer complexes {[UO₂(L_x)(OH₂)]_n (1–5) of ligands (HL_x) were prepared as follows:



{[UO₂(L₁)₂(OH₂)]_n (1). Anal. Calcd for U(C₃₄H₂₆N₆O₉) (%): C, 45.33; H, 2.89; N, 10.71; U, 26.44. Found (%): C, 45.14; H, 2.78; N, 10.50; U, 26.22.

{[UO₂(L₂)₂(OH₂)]_n (2). Anal. Calcd for U(C₃₄H₂₆N₆O₇) (%): C, 47.01; H, 3.00; N, 9.68; U, 27.42. Found (%): C, 46.89; H, 2.88; N, 9.47; U, 27.24.

{[UO₂(L₃)₂(OH₂)]_n (3). Anal. Calcd for U(C₃₂H₂₂N₆O₇) (%): C, 45.71; H, 2.62; N, 10.00; U, 28.33. Found (%): C, 45.64; H, 2.53; N, 9.78; U, 27.88.

{[UO₂(L₄)₂(OH₂)]_n (4). Anal. Calcd for U(C₃₂H₂₀N₆O₇Cl) (%): C, 42.24; H, 2.20; N, 9.24; U, 26.18. Found (%): C, 42.11; H, 2.09; N, 9.04; U, 25.77.

{[UO₂(L₅)₂(OH₂)]_n (5). Anal. Calcd for U(C₃₂H₂₀N₈O₁₁) (%): C, 53.64; H, 2.76; N, 7.54; U, 32.87. Found (%): C, 53.45; H, 2.55; N, 7.73; U, 32.57.

lected by vacuum filtration. The preparation is shown in Figure S1.

2.3 | Synthesis of the polymer complexes (1–5)

To a solution of the ligands (HL_x) (1 mmol) in mixture of 30 ml (2:1 v/v) of DMF and methanol (25 mL) solution of UO₂(NO₃)₂·6H₂O (1 mmol) was slowly added with stirring for 1 hr. The mixed solution was stirred for another ~ 2–3 hrs under reflux. The solvent was removed to a half volume after the completing of the reaction and cooled down to room temperature. The polymer complexes were

3 | RESULTS AND DISCUSSION

3.1 | Characterization of the ligands (HL_x)

It has been found that the reaction of aniline or *p*-substituted derivatives (1a) with nitrous acid (NaNO₂/HCl) afforded the diazonium salt (2a), which underwent coupling reaction with 8-hydroxy-7-quinolinecarboxaldehyde (3a) to yield the azo coupling product (HL_x). The reaction can be represented in Figure S1.

The IR spectra of the ligands (HL_x) are devoid of the bands due to the NH₂ group of the *p*-derivatives of aniline

and a band due to $-N=N-$ group, the azo dye ligands (HL_x) linkage appeared. The IR spectra of the ligands (HL_x) show a medium-broad band centered at ~ 3315 – 3325 cm^{-1} due to $\nu(\text{OH})$ and strong bands at ~ 1280 – 1295 cm^{-1} $\delta(\text{OH})$, due to intramolecular hydrogen bond.^[20] Similarly another medium intensity bands appearing at $\sim 1271 \pm 8\text{ cm}^{-1}$ in the free ligands are due to the $\nu(\text{C-O})$ stretching vibrations (Figure S2). The $\text{C}_8\text{-OH}$ group of the quinoline can form an intramolecular hydrogen bond with the aldehydic-O group (Figure S1(B)) and/or azomethine-N group (Figure S1(C)) while the other form an intermolecular hydrogen bond with the oxygen of the $\text{C}_8\text{-OH}$ group, azomethine-N or aldehyde-O of the another molecule (Figure S1(E & F)), as shown in literatures of El-Sonbati et al.^[5] The band is slightly affected by the nature and position of the substituent. The $\nu(\text{C=N})$ stretching vibration is observed in the form of a band at $\sim 1585 \pm 5\text{ cm}^{-1}$. The spectral region at ~ 1600 – 1400 cm^{-1} is complicated because of the stretching modes of $-\text{C}=\text{C}-$ and $-\text{N}=\text{N}-$ which are superimposed in the same region.

The ^1H NMR studies for the free ligands under investigation in DMSO-d_6 show 9.16–12.25 ppm are assigned to the OH protons of the quinolone ring. The existence of the OH signal at high downfield of TMS due to strong hydrogen bonding occurs between OH and the azomethine nitrogen of quinoline moiety and/or CO group as shown in Figure S1. This favors the formation of an intramolecular hydrogen bond with the CO group. The signal due to OH proton disappears in D_2O solution

attributable to the strongly hydrogen bonded. The spectra of quinoline and Ar-H rings appeared in the ~ 9.30 – 7.23 ppm . The resonance signals at ~ 2.55 and $\sim 3.85\text{ ppm}$ are due to the methyl group attached to the keto group and methoxy protons, respectively.

3.2 | Theoretical studies of ligands (HL_x) and their tautomeric forms

The geometrical structures of the ligands (HL_x) (Figure S1(A)) and their tautomeric forms (**D** and **G**) are optimized and shown in Figures 1–5. The lowest unoccupied molecular orbital energy (E_{LUMO}), the highest occupied molecular orbital energy (E_{HOMO}), the energy gap (HOMO–LUMO energy gap (ΔE)) between them values and the other quantum chemical parameters are listed in Table 1. The values of ΔE which are an important stability index, is applied to develop theoretical models for explaining the structure and conformation barriers in many molecular systems.^[30,36,37] The values of the energy gap (ΔE) for the ligands (HL_x) (Figure S1(A)) and their tautomeric forms (**D** and **G**) confirmed to that the form (**G**) is more stable than the other tautomeric forms (**A** and **D**) (Table 1). Primary calculations reveal that the tautomeric form (**G**) of ligands (HL_x) is more stable than ligands (HL_x) (Figure S1(A)) and tautomeric form (**D**). Figure 6 shows the HOMO and LUMO orbital's for tautomeric form (**G**) of ligands (HL_x). The elected bond

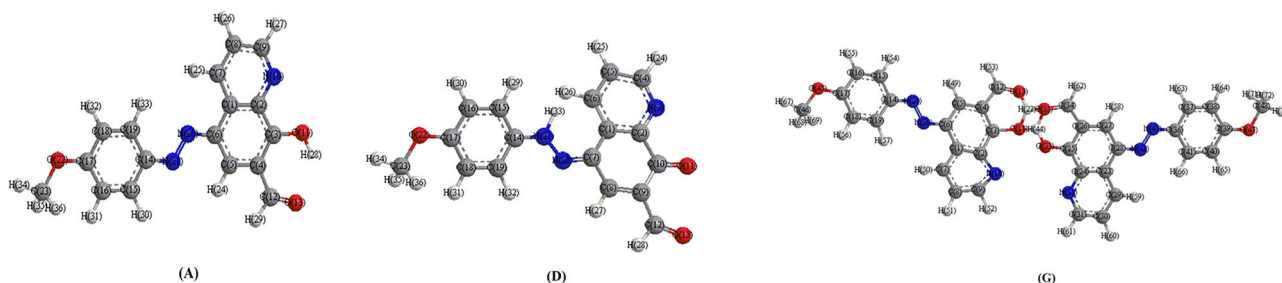


FIGURE 1 The highest occupied molecular orbital (HOMO) and the lowest unoccupied molecular orbital (LUMO) of the tautomeric form (**G**) of ligands (HL_x)

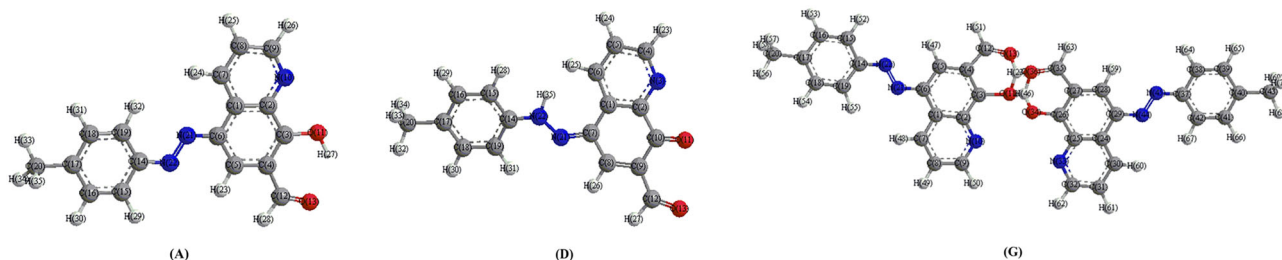


FIGURE 2 The optimized molecular structures of the HL_1 ligand and its tautomeric forms (**D** and **G**)

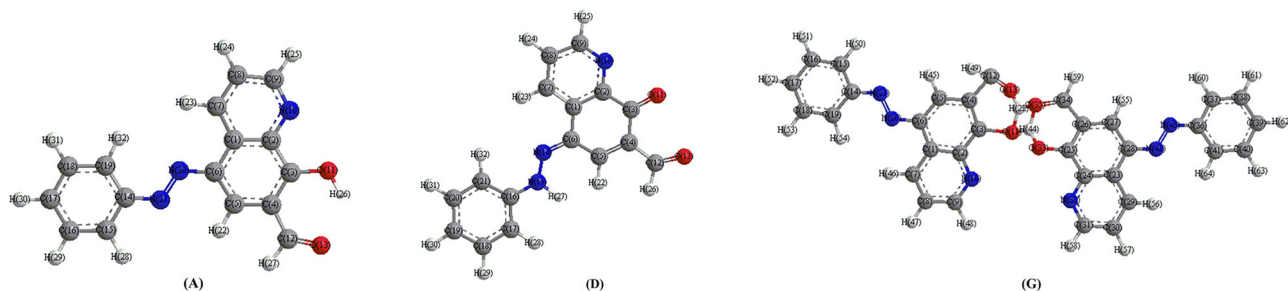


FIGURE 3 The optimized molecular structures of the HL₂ ligand and its tautomeric forms (D and G)

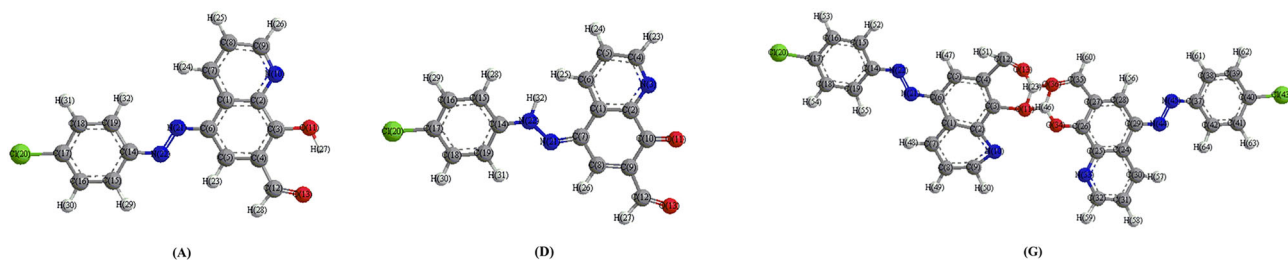


FIGURE 4 The optimized molecular structures of the HL₃ ligand and its tautomeric forms (D and G)

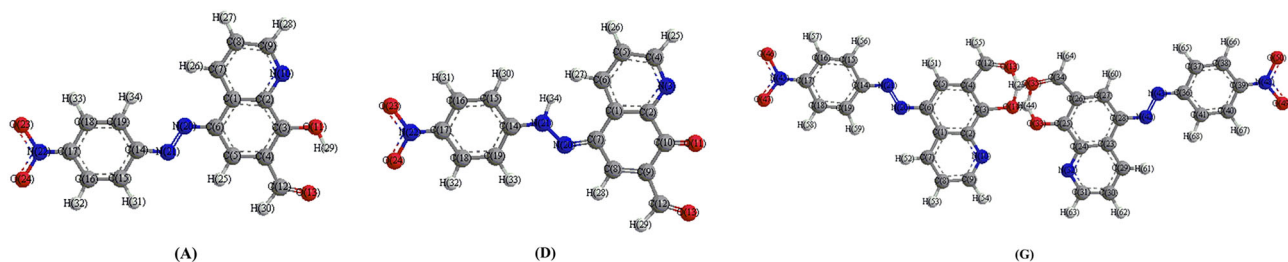


FIGURE 5 The optimized molecular structures of the HL₄ ligand and its tautomeric forms (D and G)

TABLE 1 The calculated quantum chemical parameters of the ligands (HL_x) and their tautomeric forms

Ligands ^a	Forms ^a	E _{HOMO} (eV)	E _{LUMO} (eV)	ΔE (eV)	χ (eV)	η (eV)	σ (eV) ⁻¹	Pi (eV)	S (eV) ⁻¹	ω (eV)	ΔN _{max}
HL ₁	(A)	-4.820	-4.219	0.601	4.520	0.301	3.328	-4.5195	1.664	33.986	15.040
	(D)	-7.172	-4.043	3.129	5.608	1.565	0.639	-5.6075	0.320	10.049	3.584
	(G)	-4.928	-4.370	0.558	4.649	0.279	3.584	-4.649	1.792	38.733	16.663
HL ₂	(A)	-4.961	-4.423	0.538	4.692	0.269	3.718	-4.692	1.859	40.919	17.442
	(D)	-7.175	-4.165	3.01	5.670	1.505	0.665	-5.670	0.332	10.681	3.767
	(G)	-5.219	-4.725	0.494	4.972	0.247	4.049	-4.972	2.024	50.042	20.130
HL ₃	(A)	-5.059	-4.490	0.569	4.775	0.285	3.515	-4.775	1.758	40.063	16.782
	(D)	-7.478	-4.405	3.073	5.942	1.537	0.651	-5.942	0.325	11.488	3.867
	(G)	-5.475	-4.966	0.509	5.221	0.255	3.929	-5.221	1.965	53.543	20.513
HL ₄	(A)	-4.883	-4.292	0.591	4.588	0.296	3.384	-4.588	1.692	35.609	15.525
	(D)	-7.171	-4.044	3.127	5.608	1.564	0.640	-5.608	0.319	10.056	3.587
	(G)	-5.015	-4.494	0.521	4.755	0.261	3.839	-4.755	1.919	43.388	18.251
HL ₅	(A)	-6.413	-4.574	1.839	5.494	0.920	1.088	-5.494	0.544	16.410	5.974
	(D)	-7.177	-3.880	3.297	5.529	1.649	0.607	-5.529	0.303	9.270	3.354
	(G)	-6.087	-5.314	0.773	5.701	0.387	2.587	-5.701	1.294	42.038	14.750

^aSymbols are given in Figure S1.

lengths and bond angles for tautomeric form (**G**) of ligands (HL_x) are listed in Tables S1-S5.

3.3 | Molecular docking study of tautomeric forms (**A** and **D**) of ligands (HL_x)

The molecular docking between ligands (HL_x) (Figure S1(**A**)) and their tautomeric form (**D**) with two receptors of the breast cancer (1JNX) and the prostate cancer (2Q7K) was calculated. The results showed a possible arrangement between the ligands (HL_{1-5}) (Figure S1(**A**)) and their tautomeric form (**D**) with receptors of the breast cancer (1JNX) and the prostate cancer (2Q7K).^[38-40] The molecular docking study showed a favorable interaction between the ligands (Figure S1(**A**)) and their tautomeric form (**D**) with 2Q7K and 1JNX receptors (Figures 7,8, S3 and S4) and the calculated energy is listed in Tables 2 and 3. According to the obtained results, HB plot curve for the receptor of prostate cancer (2Q7K) indicates that the ligands ($HL_{1,4}$ and 5) (Figure S1(**A**)) and tautomeric form (**D**) of ligands (HL_{1-5}) bind with hydrogen bond interactions of the protein and decomposed interaction energies (kcal/mole) where the HL_{1-5} ligands (Figure S1(**A**)) and their tautomeric form (**D**) with receptor of prostate cancer (2Q7K) as appear in Figures S5-S8. As well as the interaction for the receptors of prostate cancer (2Q7K) and breast cancer (1JNX) with the ligands (HL_x) (Figure S1(**A**)) and their tautomeric form (**D**) is possible. 2D plot curves of docking for the ligands (HL_x) (Figure S1(**A**)) and their tautomeric form (**D**) with the receptors of 2Q7K and 1JNX shown in Figures S9-S12. These interactions activate apoptosis in cells of cancer for the interactions with HL_x ligands (Figure S1(**A**)) and their tautomeric form (**D**).

The compound has higher value of estimated free energy of binding against receptor target is strong inhibitory activity. In Tables 2 and 3, the ligands (HL_x) (Figure S1(**A**)) are efficient inhibitors and the best interaction with prostate cancer (2Q7K) and breast cancer (1JNX) than the tautomeric form (**D**) of ligands (HL_x). Also, it was found that the receptor of prostate cancer (2Q7K) shows the best interaction than breast cancer (1JNX) with ligands (HL_x) (Figure S1(**A**)).

The best geometrical structure of the ligands (HL_{1-5}) (Figure S1(**A**)) is agreed well with its predicted best inhibitory effect to receptors of 2Q7K prostate cancer and 1JNX breast cancer. In addition to the data proven that, the HL_x ligands (Figure S1(**A**)) are efficient inhibitors of receptors of prostate cancer and breast cancer (1JNX) than tautomeric form (**D**) of ligands (HL_x). These

results are found to be in good agreement with the similar results were obtained recently.^[6,41]

The histogram of the HOMO-LUMO energy gap (ΔE) and the estimated free energy of binding of the receptors of breast cancer (1JNX) and the prostate cancer (2Q7K) for the ligands (HL_x) is shown in Figure 9. It is observed that the ΔE values of the ligands (HL_x) increases in the order $HL_2 < HL_3 < HL_4 < HL_1 < HL_5$.

3.4 | Infrared spectra and nature of coordination

The analytical data of the polymer complexes are in good agreement with stoichiometry proposed for polymer complexes (see Experimental part). All the polymer complexes did not melt but decompose at temperature greater than their ligands, indicating a strong bonding between the ligands and metal ion. As the reaction proceeded in the presence of DMF, the ligands dissolved completely, as shown by the color change of the reaction mixture.

The polymer complexes were obtained in low yield, possibly, due to low solubility of the ligands. The values of the molar conductance in DMF in 10^{-3} M solutions are low, suggesting a non-electrolytic nature for these polymer complexes. All polymer complexes are stable at room temperature.

The analytical data of polymer complexes (**1-5**) are presented in Experimental part. The polymer complexes are brightly colored and thermally stable. The polymer complexes are insoluble in water and common organic solvents but show solubility in DMSO and DMF. The analytical data of the polymer complexes indicate 1:2 metal-ligand stoichiometries. The azo dyes have several coordination sites but the involvement of all donor atoms in bonding to the metal on formation of a polymer complex is sterically not favorable. However, linear dimers^[42] are possible and the structure of the polymer complexes may be represented as shown in Figure S1.

The infrared spectra of the metal chelates are complex and it is not possible to assign all the bands without ambiguity. However, structurally important bonds such as those due to the ν (OH), ν (CO), ν (-N=N-) and ν (C=N) modes are distinguishable and provide inequivalent evidence regarding the structural features of the ligands and their manner of bonding with UO_2^{2+} .

On comparison of the IR spectra data of all the polymer complexes with the data of azo dye ligands, the absorption modes indicated that the azo dye ligands were principally coordinated to the uranium metal ion in tridentate matter. The coordination modes of bonding have the following remarks:

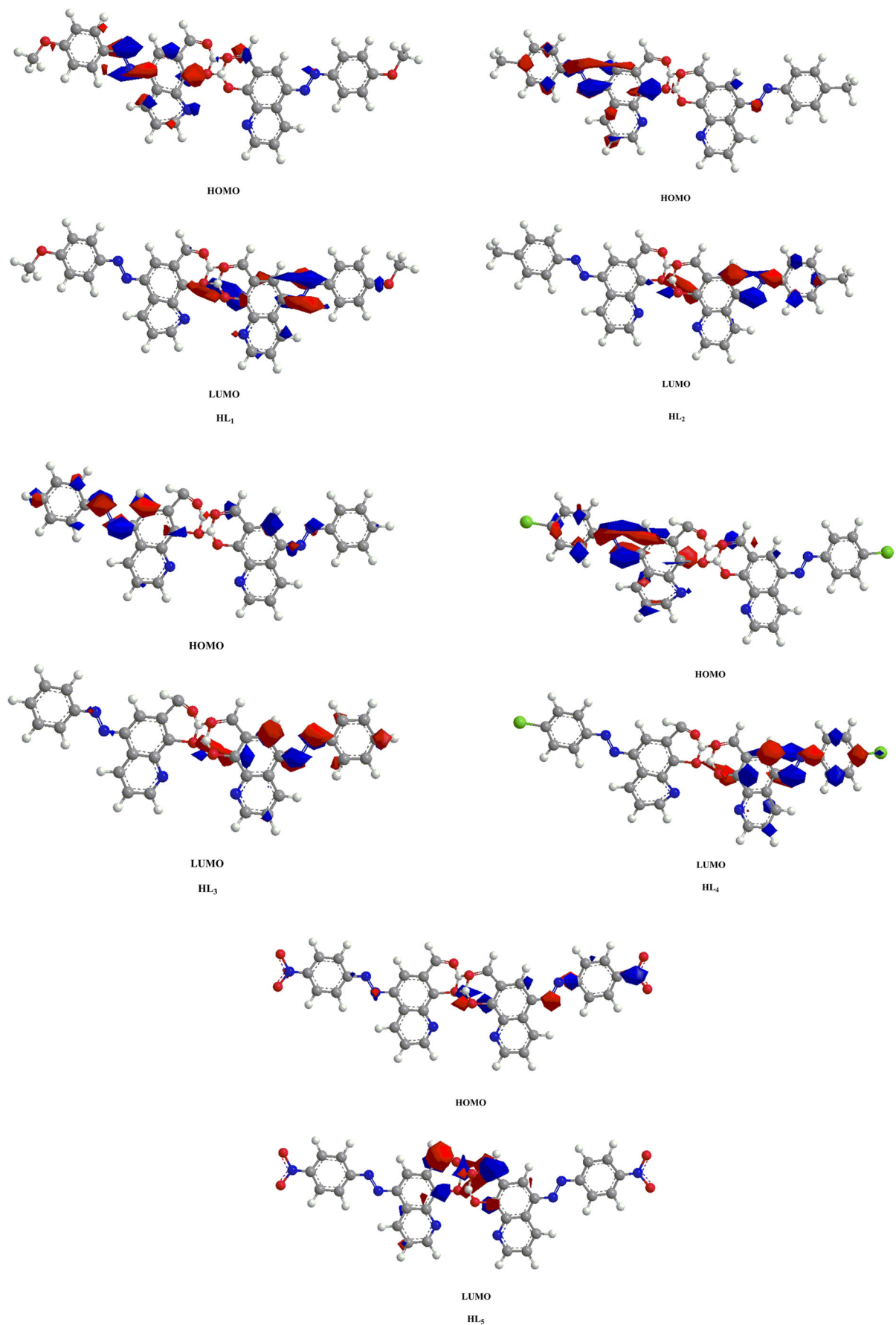


FIGURE 6 The optimized molecular structures of the HL₅ ligand and its tautomeric forms (D and G)

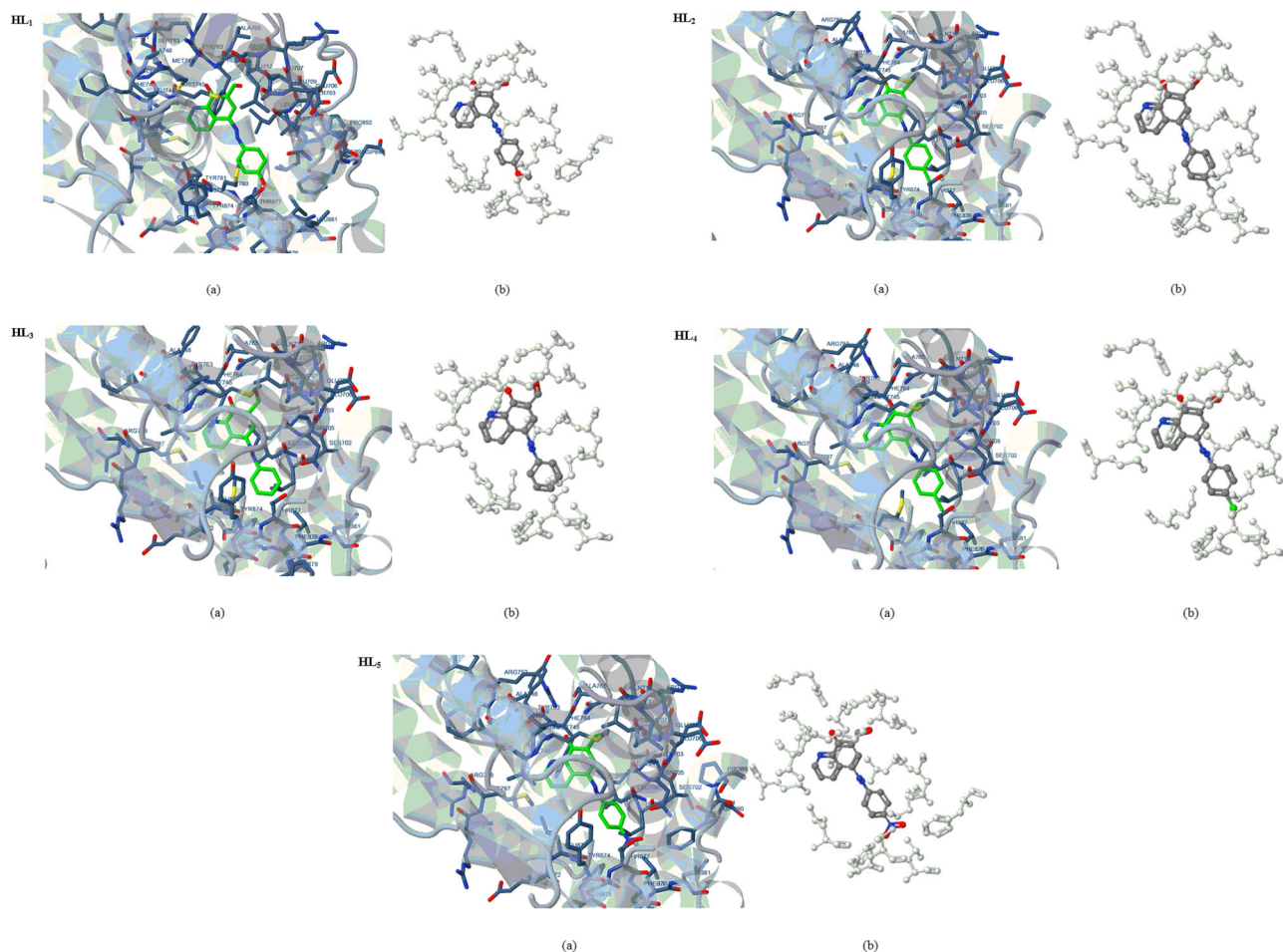


FIGURE 7 The ligands (HL_x) (green in (a) and gray in (b)) in interaction with receptor of prostate cancer (2Q7K)

1. The presence of UO_2^{2+} ion in solution exist in a tautomerism equilibrium $A \leftrightarrow B \leftrightarrow C$ (Figure S1).
2. All polymer complexes $\{[UO_2(L_x)_2(OH_2)]\}_n$ exhibit a IR broad band at $\sim 3325\text{--}3345\text{ cm}^{-1}$, attributed to ν (OH) of water molecule associated with the formation of complex as well as new bands in the regions $935\text{--}950$ and $645\text{--}650\text{ cm}^{-1}$, attributed to $\rho(H_2O)$ and $\omega(H_2O)$ of the coordinated water molecule (Figure S13).
3. All the polymer complexes show the disappearance of the ν (OH) ($3210\text{--}3325\text{ cm}^{-1}$) and δ (OH) ($1285\text{--}1295\text{ cm}^{-1}$) and the last band is replaced by a band at $1295\text{--}1315\text{ cm}^{-1}$, indicating the coordination through the oxygen atom (O^-) of the phenol group ($C_8\text{-OH}$) owing to strong hydrogen bonding in both intramolecular $[O\text{-H} \dots O, O\text{-H} \dots N]$ [Figure S1 (B & C)] and intermolecular hydrogen bonding of the $O\text{-H} \dots O$ type [Figure S1 (E & F)]. This is supported by the appearance of the characteristic band at $530\text{--}495\text{ cm}^{-1}$ due to metal-oxygen stretching vibrations in the polymer complexes.
4. All the polymer complexes showed a very strong band at $\sim 1585\text{--}1590\text{ cm}^{-1}$ characterized to pyridine $\nu(C=N)$ which upon complexation, lying at the same position, indicating that the N atom of quinoline ring does not participate in polymer complexes formation.^[43]
5. All the polymer complexes reveal IR bands due to the $\nu(-N=N-)$ group which is also observed at lower frequencies at $\sim 1570\text{--}1560\text{ cm}^{-1}$ indicating coordination through one of the nitrogen atom of the azo group (Figure S13).
6. IR bands at $\sim 1655\text{ cm}^{-1}$ ν (CO) were shifted at higher frequency in the ligands than in the respective complexes by $15\text{--}25\text{ cm}^{-1}$, revealing its involvement in UO_2^{2+} polymer complexes. The decrease of electronic density of the ring may be correlated with the donor character of the oxygen atom in the M-O bond. A correlation was observed by comparing the position of the ν (CO) band in the free ligand and the corresponding complexes indicating that the higher electronegativity provides higher shift.
7. Polymer complexes show a medium intensity band at $903\text{--}940\text{ cm}^{-1}$ and a strong band at $826\text{--}860\text{ cm}^{-1}$ due to antisymmetric and symmetric frequencies,

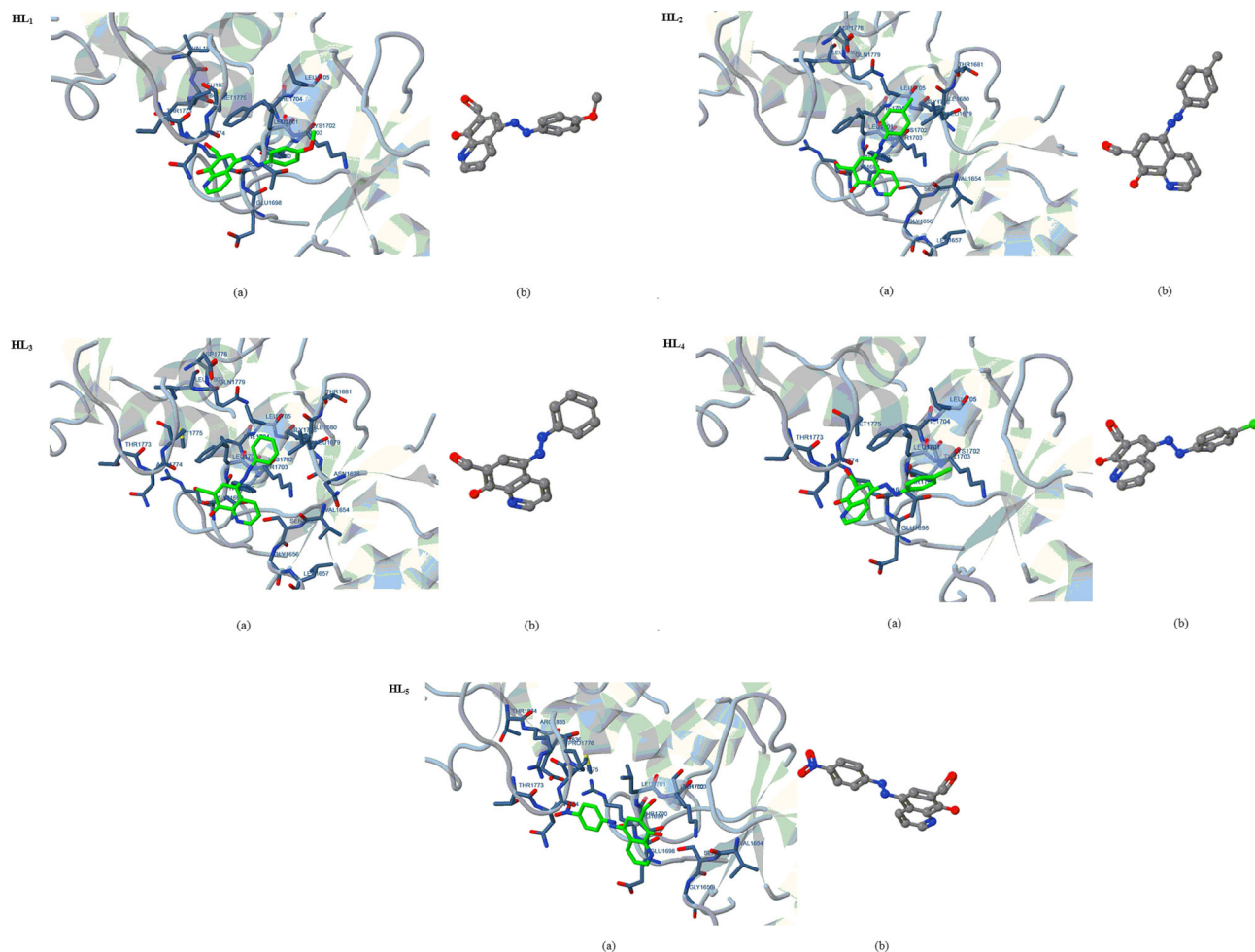


FIGURE 8 The ligands (HL_x) (green in (a) and gray in (b)) in interaction with receptor of breast cancer (1JNX)

TABLE 2 Energy values obtained in docking calculations of tautomeric forms (A and D)^a of ligands (HL_x) with receptor of prostate cancer (PDB code 2Q7K)

Ligand	Tautomeric form	Estimated free energy of binding (kcal/mol)	vdW+ bond+ desolv energy (kcal/mol)	Electrostatic Energy (kcal/mol)	Total intercooled Energy (kcal/mol)	Interact surface (Å)
HL ₁	(A)	-6.27	-6.59	-0.12	-6.72	561.289
	(D)	-4.56	-5.63	-0.11	-5.75	572.803
HL ₂	(A)	-7.80	-8.29	-0.08	-8.37	544.335
	(D)	-6.36	-7.30	-0.07	-7.37	551.696
HL ₃	(A)	-7.54	-8.26	-0.07	-8.33	516.853
	(D)	-6.16	-7.29	-0.01	-7.29	514.252
HL ₄	(A)	-6.73	-6.68	-0.12	-6.79	549.458
	(D)	-5.19	-7.71	-0.02	-7.73	523.076
HL ₅	(A)	-4.85	-5.87	-0.07	-5.95	552.421
	(D)	-4.12	-7.69	+0.06	-7.63	524.546

^aSymbols as given in Figure S1.

respectively, indicating that the moieties of UO_2^{+2} are virtually linear. IR shows bands at $500\text{--}518\text{ cm}^{-1}$ (U-O) and $400\text{--}417\text{ cm}^{-1}$ (U-N) stretching vibrations.

8. IR spectra provide an additional support for the obtained results from the by considering the changes for the NMR spectra of the UO_2^{2+} polymer complexes

TABLE 3 Energy values obtained in docking calculations of tautomeric forms (A and D)^a of ligands (HL_x) with receptor of breast cancer (PDB code 1JNX)

Ligand	Tautomeric form	Estimated free energy of binding (kcal/mol)	vdW+ bond+ desolv energy (kcal/mol)	Electrostatic Energy (kcal/mol)	Total intercooled Energy (kcal/mol)	Interact surface (Å)
HL ₁	(A)	-4.74	-5.93	-0.16	-6.10	599.611
	(D)	-4.20	-5.57	-0.02	-5.59	559.121
HL ₂	(A)	-5.28	-5.83	+0.07	-5.76	599.786
	(D)	-4.59	-5.79	-0.01	-5.81	542.572
HL ₃	(A)	-5.26	-5.83	+0.06	-5.77	578.756
	(D)	-4.48	-5.16	-0.06	-5.22	537.238
HL ₄	(A)	-4.86	-5.98	-0.07	-6.05	568.751
	(D)	-4.44	-5.61	-0.01	-5.62	551.402
HL ₅	(A)	-4.46	-5.72	-0.23	-5.95	604.349
	(D)	-4.17	-5.73	+0.10	-5.63	539.02

^aSymbols as given in Figure S1.

under investigation in comparison with those of the free ligands. For polymer complexes, the disappearance of the signal observed at 9.16–12.25 ppm in the free ligands indicates the involvement and deprotonation of the OH group in chelation. Coordinated water molecules were observed at ~ 3.49 ppm for polymer complexes.

9. Various authors^[44–49] have also correlated the basicity of the ligands in the uranyl complexes with the decrease of antisymmetric stretching frequency O=U=O (ν_3) due to the electrostatic repulsion between the non-bonding π -electrons of the uranyl oxygen and ligand–metal charge transfer electrons.

Based on the above discussion, the formed polymer complexes coordinate by the oxygen atom of the carbonyl group, oxygen atom of phenolic group and one nitrogen atom of the azo dye group are coordinated in a tridentate binuclear fashion.

3.5 | X-ray diffraction analysis of the polymer complexes

The X-ray powder diffraction of the polymer complexes (**1,3** and **4**) are represented in Figure S14. The XRD patterns show the broad peaks in the range $2\theta = 18^\circ - 25^\circ$ indicating amorphous structures for the polymer complexes.

3.6 | Thermal studies

The TGA and Dr TGA curves of the polymer complexes (**1–4**) are measured from 30 °C to 800 °C with heat flow 15 °C/min and shown in Figure 10. The TGA curves of

the polymer complexes show two degradation steps. The first step beginning at ~ 40 °C is due to the loss of uncoordinated water molecules. The second step shows loss of organic ligand. At temperatures above 500 °C UO₃ is formed then gives U₃O₈.^[50,51] TGA studies can be used to explain the structure of the complexes as well as determining the nature of the coordinated molecules. From TGA analyses, it was found that the UO₂(II) polymer complexes (**1–4**) under investigation are more stable than the ligand.

3.7 | Kinetic calculations

Coats-Redfern and Horowitz-Metzger methods^[52,53] were used for the determination of the thermodynamic parameters for polymer complexes (**1–4**). The enthalpy (ΔH^*) and Gibbs free energy change of the decomposition (ΔG^*) were calculated from the well-known equations $\Delta H^* = E_a - RT$ and $\Delta G^* = \Delta H^* - T\Delta S^*$, respectively, as well as the thermal activation energy for decomposition (E_a) and entropy (ΔS^*).

The calculated values of E_a , ΔH^* , ΔS^* and ΔG^* of the decomposition stages for polymer complexes (**1–4**) are listed in Table 4 and shown in Figures S15 and S16. The thermodynamic data obtained from Coats-Redfern and Horowitz-Metzger methods are comparable and can be considered in good agreement with each other.^[25,54] The entropy is found to be negative values for polymer complexes (**1–4**) which indicates more ordered activated complex than the reactants or the reaction is slow.^[32,54] The entropy reflects the thermal stability of the compounds. The positive value of ΔG^* for the polymer complexes (**1–4**) indicates that the process is non-spontaneous.

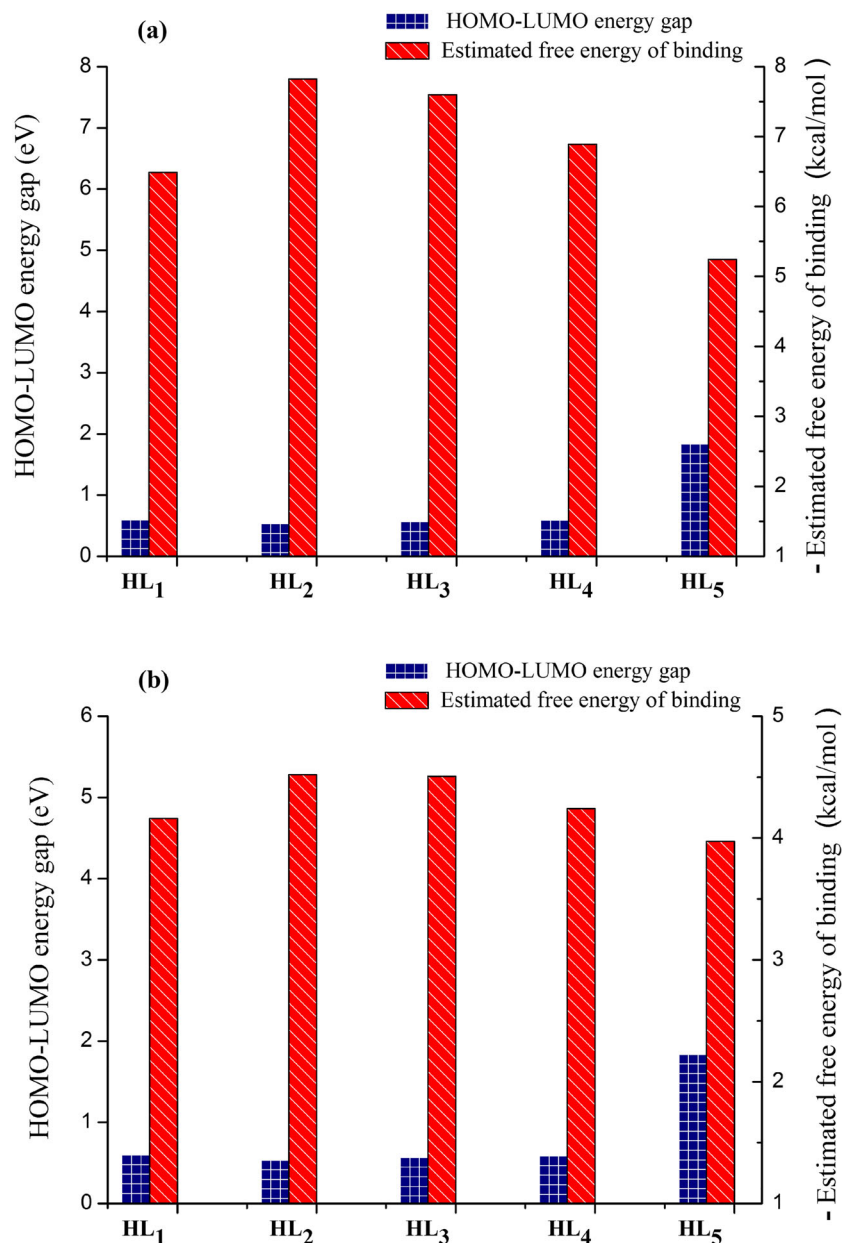


FIGURE 9 The histogram of the HOMO–LUMO energy gap (ΔE) and the estimated free energy of binding for the ligands (HL_{*x*}) where (a) receptor of prostate cancer (PDB code 2Q7K) and (b) receptor of breast cancer (PDB code 1JNX)

3.8 | Determination of the bond lengths of uranyl ion in polymer complexes

It may be assumed that the uranyl ion UO_2^{2+} is linear. Although such linearity may not be deduced completely unambiguously from any experiment. There is general accord that a collinear O–U–O structure affords the better interpretation of the Raman infrared and electronic spectra and x-ray diffraction intensities. It is also rather well established^[31] that the uranyl ion possesses three characteristic IR frequencies: the symmetric stretching frequency, ν_1 or σ_g^+ , lying in the range $780\text{--}900\text{ cm}^{-1}$; the asymmetric stretching frequency, ν_3 or (σ_u^+) , lying in the range $800\text{--}1000\text{ cm}^{-1}$; and the bending vibration, ν_2 or π_u , appearing in the neighborhood of 200 cm^{-1} . The rather large frequency intervals quoted for symmetric ν_1

and antisymmetric stretching frequencies (ν_3) are indicative of the fact that appropriate complexation of the uranyl ion by ligand groups presumed to lie in, or nearly in, a plane perpendicular to the axial O–U–O direction, produce extremely large variations in ν_1 and ν_3 this latter is evident from the compilation of Table S6. It is also known that similar large variations in the metal–oxygen stretching frequencies of other HL_{*x*} ligands are occasioned by change of ligation.^[31] It has also observed that the uranyl stretching frequencies seem to decrease as one proceeds from left to right along the spectrochemical series. The antisymmetric stretching frequency (ν_3) values decrease as the donor characteristics increase as is observed for *p*-electron-releasing substituents, where the basicity of the donating atom increases. The experimental results reveals an excellent linear relation between ν_1 and

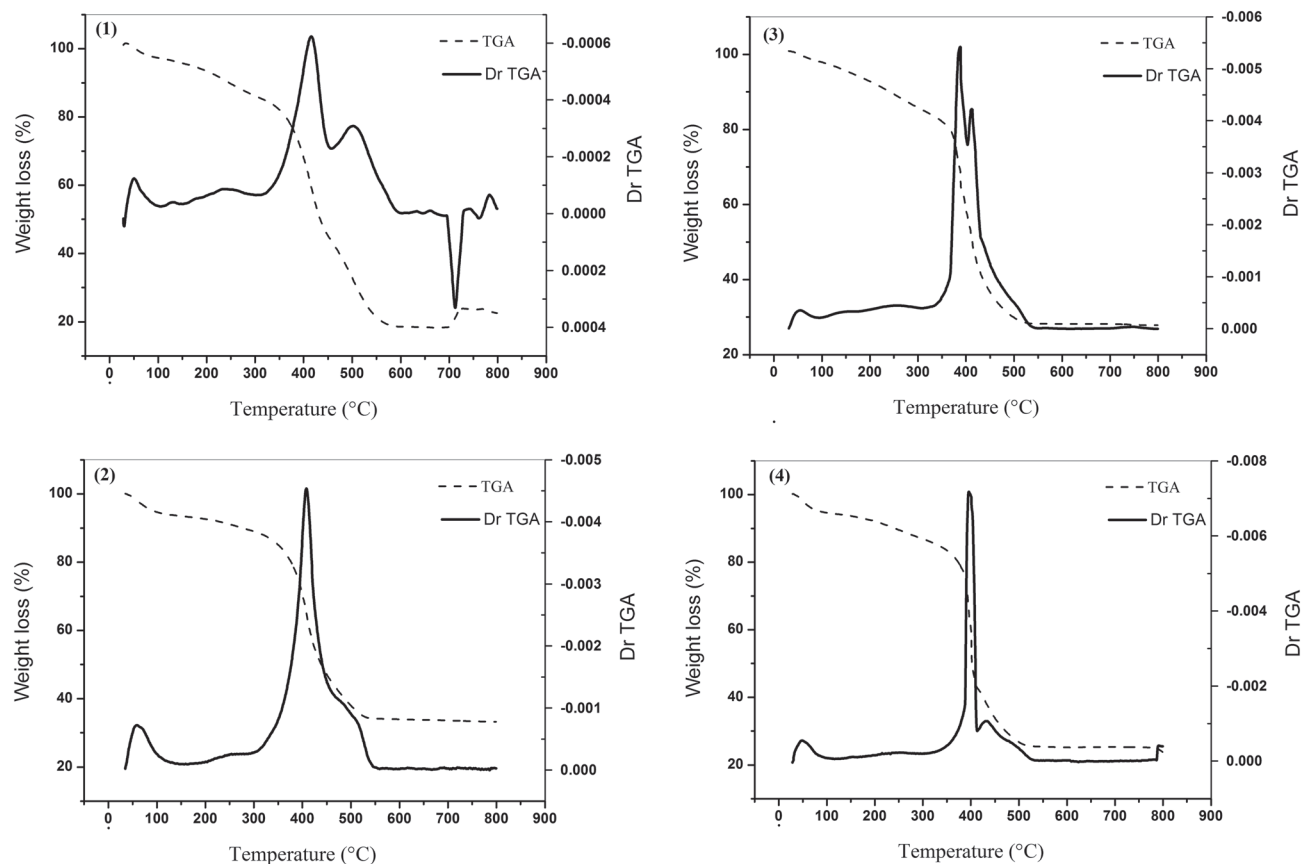


FIGURE 10 TGA curves and Dr TGA of polymer complexes

TABLE 4 Thermodynamic activation energy for polymer complexes

Complex ^a	Decomposition temperature (°C)	Method	Parameter			
			E _a (kJ mol ⁻¹)	ΔS [*] (J mol ⁻¹ K ⁻¹)	ΔH [*] (kJ mol ⁻¹)	ΔG [*] (kJ mol ⁻¹)
(1)	170–330	CR	50.1	−2.05E+02	45.8	153
		HM	60.7	−1.79E+02	56.3	150
	330–440	CR	152	−7.11E+01	147	194
		HM	164	−4.36E+01	158	187
(2)	200–330	CR	61.7	−1.87E+02	57.2	158
		HM	72	−1.60E+02	67.6	154
	330–420	CR	167	−4.49E+01	162	191
		HM	180	−1.27E+01	175	183
(3)	190–400	CR	41.7	−1.91E+02	37.2	140
		HM	44.9	−2.14E+02	40.4	156
	400–530	CR	156	−6.58E+01	150	199
		HM	168	−7.09E+01	162	215
(4)	150–330	CR	42.5	−2.20E+02	38.2	151
		HM	50.9	−1.96E+02	46.7	147
	330–410	CR	183	−2.32E+01	178	193
		HM	198	1.77E+01	193	181

^aNumbers as given in Experimental part.

ν_3 with the slope corresponding to $(1 + 2M_O/M_U)^{1/2}$ (M_O and M_U are the masses of oxygen and uranium atoms, respectively, (Figure 11a)). Similar results have been reported by McGlynn and Smith.^[55] Instead of the linear

relation between ν_1 and ν_3 frequencies, the El-Sonbati equation^[44] has focused attention on their normalized differences, in which such differences do not depend on the masses of oxygen and/or uranium atoms.

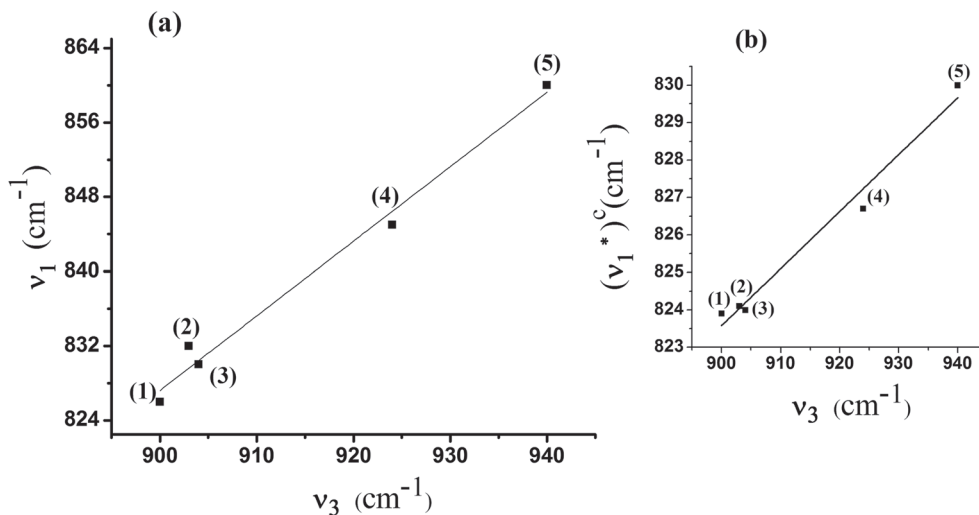


FIGURE 11 The relation between a) ν_3 vs. ν_1 and b) ν_3 vs. $(\nu_1^*)^c$ for polymer complexes

It is the purpose of this paper to show how using the El-Sonbati equation from which the U-O bond force constant should eventually serve as a fairly accurate measure of the U-O bond distance in given compounds. The force constant for the U-O bond [$F_{U-O} 10^{-8}$ (N/Å)], (F_{U-O}^s), (F_{U-O}^o), the U-O bond distance (r_{U-O} (Å)) and spectral data used herein are summarized in Table S6. It is apparent from Table S6 that a plot of $\nu_1 + \nu_3$ and/or ν_3 vs. force constant for the U-O [$F_{U-O} 10^{-8}$ (N/Å) or $F_{U-O}^x 10^{-8}$ (N/Å)] and the U-O bond distance (r_{U-O} (Å) or r_{U-O} (Å)) gives a straight line with an increase in the value of $\nu_1 + \nu_3$ and/or ν_3 decrease r_{U-O} and an increase in the force constant of the U-O bond as shown in Figures 12,13 and S17-S19. There is also a straight line relationship between r_{U-O} and p -substituent, Hammett's constant (σ^R) with negative slope, i.e., the higher the value of the R, the lower r_{U-O} and

the higher the force constant of the U-O bond (Figures 14, S20 and S21). Also, plotting of r_1 , r_2 , r_3 , and r_t (bond distance, r_{U-O}) vs. ν_3 gives straight lines with increase in the value of ν_3 and decrease in r_{U-O} (Figure S22). Our results also showed an inverse relationship between ν_3 and r_{U-O} . This can be explained by the fact that the electron-withdrawing p -substitution increases the positive charge on the UO_2^{2+} leading to an increase in ν_3 and F_{U-O} and subsequently a decrease in r_{U-O} . Accordingly, r_{U-O} values can be arranged in the following order: $p-OCH_3 > p-CH_3 > H > p-Cl > p-NO_2$, was achieved in consistent with the positive charge on the UO_2^{2+} . The plot of Hammett's substituent coefficients (σ^R) vs. a) r_1 (Å) and b) F_{U-O} (10^{-8} (N/Å)) of UO_2^{2+} complexes (1-5) (Figures 14, S20 and S21) shows all these F_{U-O} values increase with increasing σ^R while r_1 values decrease with

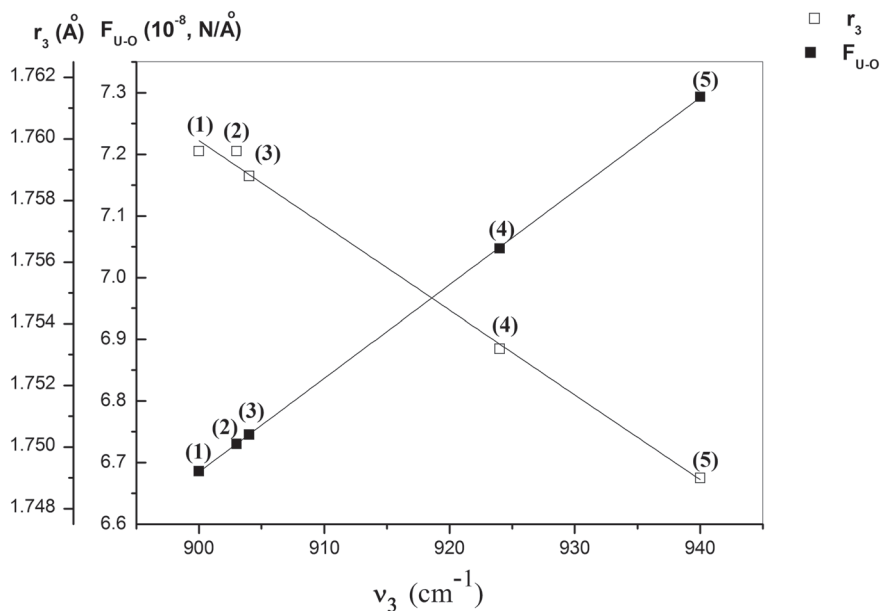


FIGURE 12 The relation r_3 (Å) and F_{U-O} (10^{-8} (N/Å)) with ν_3 (cm⁻¹) for polymer complexes

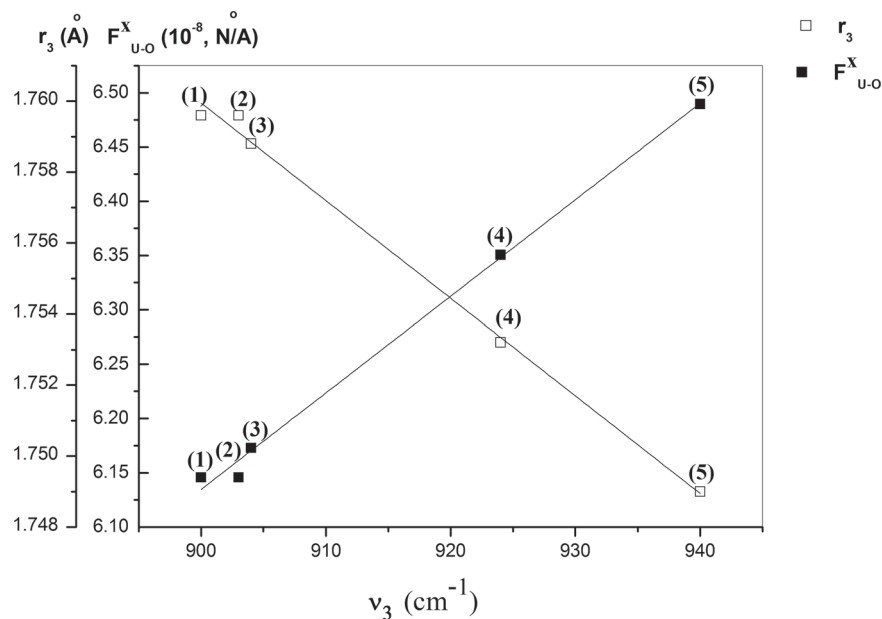


FIGURE 13 The relation r_3 (Å) and F_{U-O} (10^{-8} (N/Å)) with ν_3 (cm^{-1}) for polymer complexes

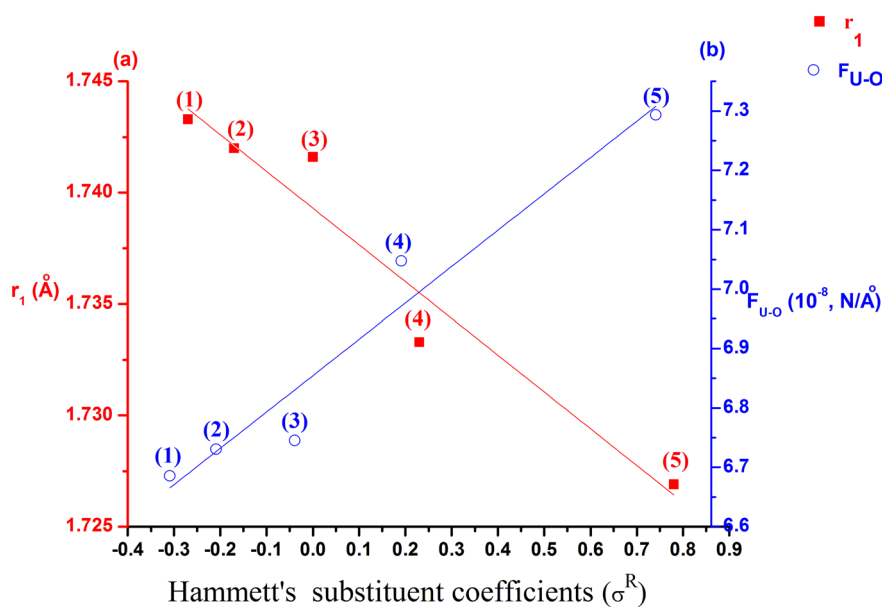


FIGURE 14 The relation between Hammett's substituent coefficients (σ^R) vs. a) r_1 (Å) and b) F_{U-O} (10^{-8} (N/Å)) of polymer complexes

increasing σ^R , this can be attributed to the fact that the charge effectively increased due to the electron withdrawing substituent in complexes (4 & 5), while it decreased by electrons donating character of complexes (1 & 2). This is in accordance with that expected from Hammett's constant (σ^R). These data can be explained by El-Sonbati equation^[44] for calculating the symmetric stretching frequency (ν_1^x). The (ν_1^x) data served as an accurate evaluation to the (F_{U-O}) and (r_{U-O}). There is also a straight line relationship between (ν_1^x) and (ν_3) (O=U=O) (Figure 11 b). Perhaps a new light can be shed on the problem by looking at the values of r_1 , r_2 and r_3 from a different point of view. It might be worthwhile to focus attention on

their normalized differences. Thus a new relationship between them with respect to r_t was determined by Global error which shows that the excellent validity is in the sequence: $\sqrt{(r_3-r_t)^2}$ (0.0062) > $\sqrt{(r_1-r_t)^2}$ (0.0353) > $\sqrt{(r_2-r_t)^2}$ (0.0906) for the force constant F_{U-O} and bond length, r_{U-O} of the uranyl polymer complexes. Due to small scattering power of the oxygen atom, report of the determination of U–O bond length of some uranyl complexes by X-ray study is inadequate. From the IR spectra, the stretching and interaction force constants of the complexes have been calculated.^[31,45–49] The data were used to evaluate the U–O bond distances using Badger's formula, Jones equation^[47,48] and El-Sonbati

equation.^[44] The data are quite close to the results reported earlier for other uranyl complexes.^[44,49] The variation of bond length in the complexes is due to the presence of electron releasing or electron withdrawing substituents in the equatorial position.

4 | CONCLUSION

The $\{[UO_2(L_x)(OH_2)]\}_n$ polymer complexes (**1–5**) of azo dye ligands 5(4'-derivatives phenylazo)-8-hydroxy-7-quinolinecarboxaldehyde (HL_x) were prepared and characterized by elemental analysis, 1H NMR, IR spectra, thermal analysis and X-ray diffraction analysis. Based on the above discussion, the ligands (HL_x) are monobasic and the formed polymer complexes coordinate by the oxygen atom of the carbonyl group, oxygen atom of phenolic group and one nitrogen atom of the azo dye group are coordinated in a tridentate binuclear fashion. Molecular docking of the binding between the form (**A**) of HL_x and their tautomeric form (**D**) with two receptors of the breast cancer (1JNX) and the prostate cancer (2Q7K) was discussed. It was found that the receptor of prostate cancer (2Q7K) shows the best interaction than breast cancer (1JNX) with ligands (HL_x) than tautomeric form (**D**) of ligands (HL_x). Also, it was found that the best geometrical structure of the ligands (HL_x) agreed well with its predicted best inhibitory effect to receptors of prostate cancer and breast cancer. It was found that the F_{U-O} values increase with increasing σ^R while r_1 values decrease with increasing σ^R . In case F_{U-O} values increase with increasing Hammett's substituent coefficients (σ^R), this can be attributed to the fact that the charge effectively increased due to the electron withdrawing substituent in $UO_2(II)$ polymer complexes (**4**) and (**5**), while it decreased by electrons donating character of $UO_2(II)$ polymer complexes (**1**) and (**2**). This is in accordance with that expected from Hammett's constant (σ^R).

ORCID

M.A. Diab  <https://orcid.org/0000-0002-9042-1356>

A.Z. El-Sonbati  <https://orcid.org/0000-0001-7059-966X>

Sh.M. Morgan  <https://orcid.org/0000-0002-8921-4894>

REFERENCES

- [1] S. T. Hazeldine, L. Polin, J. Kushner, K. White, T. H. Corbett, J. Biehl, J. P. Horwitz, *Bioorg. Med. Chem.* **2005**, *13*, 1069.
- [2] L. Savini, L. Chiasserini, C. Pellerano, W. Filippelli, G. Falcone, *Farmacoterapia* **2001**, *56*, 939.
- [3] M. Normand-Bayle, C. Bénard, V. Zouhiri, J. Mouscadet, H. Leh, C. Thomas, G. Mbemba, D. Desmaële, J. d'Angelo, *Bioorg. Med. Chem. Lett.* **2005**, *15*, 4019.
- [4] R. Vlahov, J. St. Parushev, P. N. Vlahov, G. Snatzke, *Pure Appl. Chem.* **1990**, *62*, 1303.
- [5] A. Z. El-Sonbati, M. A. Diab, A. M. Eldesoky, Sh. M. Morgan, O. L. Salem, *Appl. Organomet. Chem.* **2019**, *33*, e4839.
- [6] A. Z. El-Sonbati, M. A. Diab, G. G. Mohamed, M. A. Saad, Sh. M. Morgan, S. E. A. El-Sawy, *Appl. Organomet. Chem.* **2019**, *33*, e4973.
- [7] K. B. Patel, G. J. Kharadi, K. S. Nimavat, *J. Chem. Pharm. Res.* **2012**, *4*, 2422.
- [8] R. T. Bronson, M. Montalti, L. Prodi, N. Zaccheroni, R. D. Lamb, N. K. Dalley, R. M. Izatt, J. S. Bradshaw, P. B. Savage, *Tetrahedron* **2004**, *60*, 11139.
- [9] G. De Armas, M. Miró, A. Cladera, J. M. Estela, V. Cerdà, *Anal. Chim. Acta* **2002**, *455*, 149.
- [10] M. I. Abou-Dobara, N. F. Omar, M. A. Diab, A. Z. El-Sonbati, Sh. M. Morgan, O. L. Salem, A. M. Eldesoky, *Mater. Sci. Eng. C* **2019**, *103*, 109727.
- [11] M. Albrecht, K. Witt, R. Frohlich, O. Kataeva, *Tetrahedron* **2002**, *58*, 56.
- [12] K. D. Patel, H. S. Patel, *Pharm. Lett.* **2011**, *3*, 356.
- [13] D. A. Pearce, N. Jotterand, I. S. Carrico, B. Imperiali, *J. Am. Chem. Soc.* **2001**, *123*, 5160.
- [14] A. Z. El-Sonbati, M. A. Diab, M. M. El-Halawany, N. E. Salam, *Met. Chem. Phys.* **2010**, *123*, 439.
- [15] A. Z. El-Sonbati, M. A. Diab, Sh. M. Morgan, *J. Mol. Liq.* **2017**, *225*, 195.
- [16] Sh. M. Morgan, M. A. Diab, A. Z. El-Sonbati, *Appl. Organomet. Chem.* **2018**, *32*, e4305.
- [17] Sh. M. Morgan, M. A. Diab, A. Z. El-Sonbati, *Appl. Organomet. Chem.* **2018**, *32*, e4281.
- [18] Sh. M. Morgan, N. A. El-Ghamaz, M. A. Diab, *J. Mol. Struct.* **2018**, *1160*, 227.
- [19] A. Z. El-Sonbati, M. A. Diab, A. A. M. Belal, Sh. M. Morgan, *Spectrochim. Acta A* **2012**, *99*, 353.
- [20] N. A. El-Ghamaz, M. A. Diab, A. Z. El-Sonbati, O. L. Salem, *Spectrochim. Acta A* **2011**, *83*, 61.
- [21] N. A. El-Ghamaz, M. A. Diab, A. Z. El-Sonbati, Sh. M. Morgan, O. L. Salem, *Chem. Pap.* **2017**, *71*, 2417.
- [22] A. Z. El-Sonbati, A. A. M. Belal, M. S. El-Gharib, Sh. M. Morgan, *Spectrochim. Acta A* **2012**, *95*, 627.
- [23] N. A. El-Ghamaz, A. Z. El-Sonbati, Sh. M. Morgan, *J. Mol. Struct.* **2012**, *1027*, 92.
- [24] M. I. Abou-Dobara, A. Z. El-Sonbati, Sh. M. Morgan, *World J. Microbiol. Biotechnol.* **2013**, *29*, 119.
- [25] Sh. M. Morgan, A. Z. El-Sonbati, M. A. El-Mogazy, *Appl. Organomet. Chem.* **2018**, *32*, e4264.
- [26] A. I. Shah, H. M. Shukla, P. J. Shah, D. S. Raj, *Elixir Chem. Phys.* **2012**, *44*, 7378.
- [27] M. Bankova, N. Manolova, N. Markova, T. Radoucheva, K. Deilova, I. Rashkova, *Eur. Polym. J.* **1998**, *34*, 247.
- [28] P. W. Selwood, *Magnetic Chemistry*, Interscience Pub. Inc., New York **1956**.
- [29] A. Z. El-Sonbati, M. A. Diab, Sh. M. Morgan, A. M. Eldesoky, M. Z. Balboula, *Appl. Organomet. Chem.* **2018**, *32*, e4207.

- [30] Sh. M. Morgan, A. Z. El-Sonbati, H. R. Eissa, *J. Mol. Liq.* **2017**, *240*, 752.
- [31] A. Z. El-Sonbati, M. A. Diab, Sh. M. Morgan, H. A. Seyam, *J. Mol. Struct.* **2018**, *1154*, 354.
- [32] A. Z. El-Sonbati, M. A. Diab, Sh. M. Morgan, M. A. El-Mogazy, *Appl. Organomet. Chem.* **2018**, *32*, e4530.
- [33] H. M. Refaat, H. A. El-Badway, Sh. M. Morgan, *J. Mol. Liq.* **2016**, *220*, 802.
- [34] G. G. Mohamed, A. A. El-Sherif, M. A. Saad, S. E. A. El-Sawy, Sh. M. Morgan, *J. Mol. Liq.* **2016**, *223*, 1311.
- [35] M. A. Diab, A. Z. El-Sonbati, Sh. M. Morgan, M. A. El-Mogazy, *Appl. Organomet. Chem.* **2018**, *32*, e4378.
- [36] M. A. Diab, A. Z. El-Sonbati, N. A. El-Ghamaz, Sh. M. Morgan, O. El-Shahat, *Eur. Polym. J.* **2019**, *115*, 268.
- [37] A. Z. El-Sonbati, W. H. Mahmoud, G. G. Mohamed, M. A. Diab, Sh. M. Morgan, S. Y. Abbas, *Appl. Organomet. Chem.* **2019**, *33*, e5048.
- [38] Sh. M. Morgan, M. A. Diab, A. Z. El-Sonbati, *Appl. Organomet. Chem.* **2018**, *32*, e4504.
- [39] M. Kabešová, R. Boča, M. Melník, D. Valigura, M. Dunaj-Jurčo, *Coord. Chem. Rev.* **1995**, *140*, 115.
- [40] M. A. Diab, G. G. Mohamed, W. H. Mahmoud, A. Z. El-Sonbati, Sh. M. Morgan, S. Y. Abbas, *Appl. Organomet. Chem.* **2019**, *33*, e4945.
- [41] M. I. Abou-Dobara, N. F. Omar, M. A. Diab, A. Z. El-Sonbati, Sh. M. Morgan, M. A. El-Mogazy, *J. Cell. Biochem.* **2019**, *120*, 1667.
- [42] N. V. Thakkar, S. Z. Bootwala, *Synth. React. Inorg. Met.-Org. Chem.* **1996**, *26*, 1063.
- [43] J. Bassett, R. C. Denney, G. H. Jeffery, J. Mendham, *Vogel's Textbook of Quantitative Inorganic Analysis*, fourth ed., Longmans, London **1978**.
- [44] A. Z. El-Sonbati, *Spectrosc. Lett.* **1997**, *30*, 459.
- [45] A. Z. El-Sonbati, M. A. Diab, M. S. El-Shehawy, *M. Moqbal, Spectrochim. Acta A* **2010**, *75*, 394.
- [46] A. Z. El-Sonbati, A. El-Dissouky, *Transition Met. Chem.* **1986**, *12*, 112.
- [47] R. M. N. Badger, *J. Chem. Phys.* **1935**, *3*, 710.
- [48] L. H. Jones, *Spectrochim. Acta A* **1958**, *395*, *10*. **1959**, *11*, 409
- [49] S. P. McGlynn, J. K. Smith, W. C. Neely, *J. Chem. Phys.* **1961**, *35*, 105.
- [50] G. Siracusa, A. Seminara, V. Cucjnotta, S. Gurreri, *Thermochim. Acta* **1978**, *23*, 109.
- [51] L. Abate, F. Castelli, G. Siracusa, *Thermochim. Acta* **1980**, *41*, 87.
- [52] A. W. Coats, J. P. Redfern, *Nature* **1964**, *201*, 68.
- [53] H. H. Horowitz, G. Metzger, *Anal. Chem.* **1963**, *35*, 1464.
- [54] A. Z. El-Sonbati, M. A. Diab, Sh. M. Morgan, M. Z. Balboula, *Appl. Organomet. Chem.* **2018**, *32*, e4059.
- [55] S. P. McGlynn, J. K. Smith, *J. Mol. Spectrosc.* **1961**, *6*, 166.

SUPPORTING INFORMATION

Additional supporting information may be found online in the Supporting Information section at the end of the article.

How to cite this article: Diab MA, Nozha SG, El-Sonbati AZ, El-Mogazy MA, Morgan ShM. Polymer complexes. LXXVIII. Synthesis and characterization of supramolecular uranyl polymer complexes: Determination of the bond lengths of uranyl ion in polymer complexes. *Appl Organometal Chem.* 2019;e5153. <https://doi.org/10.1002/aoc.5153>